Synthesis and Biodistribution of ^{11}C-GW7845, a Positron-Emitting Agonist for Peroxisome Proliferator–Activated Receptor-γ

William B. Mathews, PhD[1]; Catherine A. Foss, PhD[1]; Doris Stoermer, PhD[2]; Hayden T. Ravert, PhD[1]; Robert F. Dannals, PhD[1]; Brad R. Henke, PhD[3]; and Martin G. Pomper, MD, PhD[1]

[1]Department of Radiology, Johns Hopkins University, Baltimore, Maryland; [2]Guilford Pharmaceuticals, Baltimore, Maryland; and [3]Research and Development, GlaxoSmithKline, Research Triangle Park, North Carolina

The goal of this study was to synthesize and evaluate in vivo the peroxisome proliferator–activated receptor-γ (PPARγ) agonist ^{11}C-GW7845 ((*S*)-2-(1-carboxy-2-{4-[2-(5-methyl-2-phenyloxazol-4-yl)ethoxy]phenyl}ethylamino)benzoic acid methyl ester) (^{11}C-compound 1). PPARγ is a member of a family of nuclear receptors that plays a central role in the control of lipid and glucose metabolism. Compound 1 is an analog of tyrosine (inhibitor constant, 3.7 nmol/L), which is an inhibitor of experimental mammary carcinogenesis. **Methods:** Protection of the carboxylic acid moiety of compound 1 was effected by treatment with *N,N*-dimethylformamide di-*tert*-butyl acetal to provide compound 2. Hydrolysis of the carbomethoxy group of compound 2 provided the benzoic acid (compound 3) that served as an immediate precursor to radiolabeling. Compound 3 underwent treatment with ^{11}C-methyl iodide followed by high-performance liquid chromatography to produce a radioactive peak sample that coeluted with a standard sample of compound 1. Analysis of biodistribution was undertaken by injecting male CD-1 mice via the tail vein with 6.03 MBq (163 μCi, 2.55 μg/kg) of ^{11}C-compound 1. To determine the tumor uptake of the radiotracer, 6 female SCID mice bearing MCF-7 xenografts were injected via the tail vein with 10.5 MBq (283 μCi, 0.235 μg/kg) of ^{11}C-compound 1. **Results:** ^{11}C-Compound 1 was synthesized at an 8% radiochemical yield in 29 min with an average specific radioactivity of 1,222 GBq/μmol (33,024 mCi/μmol; $n = 6$) at the end of synthesis. Spleen (target)-to-muscle uptake and tumor-to-muscle uptake ratios were 3.1 and 1.5, respectively, but this uptake could not be blocked with unlabeled compound 1 at 2 mg/kg. **Conclusion:** Further structural modification, perhaps to generate a less lipophilic tyrosine analog, will be necessary to enable receptor-mediated PPARγ imaging by this class of agents.

Key Words: ^{11}C-GW7845; PET; PPARγ; synthesis; biodistribution

J Nucl Med 2005; 46:1719–1726

Peroxisome proliferator–activated receptor-γ (PPARγ) is an isoform of a family of receptors that contains the classic domain structure of other (steroid and thyroid hormone) nuclear receptors (*1*). PPARγ mediates a variety of metabolic processes, including glucose and lipid homeostasis (*2*), tissue response to inflammation (*3*), and growth inhibition and apoptosis of neoplastic cells (*4*). Agonists for PPARγ may be cardioprotective (*5*) and may prevent atherosclerosis (*6*). Our interest in PPARγ stems from the ability of synthetic agonists and, in some cases, antagonists to inhibit tumor growth in vivo (*7,8*). Those findings suggest that sufficient PPARγ density may exist within certain tumors to enable ligands with adequate receptor-binding affinities to be fashioned into imaging agents for PET. A PPARγ-based PET radiopharmaceutical would allow the segregation of cancer patients into appropriate treatment groups, that is, to reveal those who might have tumors harboring the highest concentrations of receptors, thereby conferring an increased likelihood of a response to PPARγ-based hormone therapy.

Compounds of the thiazolidinedione class of PPARγ agonists are currently in clinical use for the treatment of type 2 diabetes (*9*). Indole 5-carboxylic acids and phenylpropanoic acids also have been identified as potent PPARγ agonists with affinities at least equal to those of the thiazolidinediones (*1*). Kim et al. recently reported the syntheses of 2 ^{18}F-labeled phenylpropanoic acids as potential imaging agents for PPARγ; however, neither demonstrated receptor-mediated uptake (*10*). Although those workers conceded that developing imaging agents based on PPARγ would be challenging, primarily because of poor pharmacokinetics, they suggested that imaging agents based on the newly described tyrosine-benzophenone class may prove superior because of their very high potencies. Here we describe the radiochemical synthesis and rodent biodistribution of ^{11}C-compound 1, a radiolabeled analog of a potent (inhibitor constant, 3.7 nmol/L) tyrosine-based PPARγ agonist (GW7845) that has been shown to inhibit experimental mammary carcinogenesis (*7*).

Received Apr. 13, 2005; revision accepted Jun. 27, 2005.

For correspondence or reprints contact: Martin G. Pomper, MD, PhD, Department of Radiology, Johns Hopkins University, 600 N. Wolfe St., Phipps B-100, Baltimore, MD 21287-2182.

E-mail: mpomper@jhmi.edu

MATERIALS AND METHODS

General

GW7845 was provided by GlaxoSmithKline (*9*). All chemicals and solvents were of American Chemical Society or high-performance liquid chromatography (HPLC) purity and were used as received. *N*,*N*-Dimethylformamide (DMF) was purified by overnight stirring with barium oxide and distilled before use. ^{11}C-Methyl iodide was produced by use of a PETtrace MeI Microlab (General Electric). The HPLC system consisted of 2 model 590EF pumps (Waters), 2 model 7126 injectors (Rheodyne), an in-line model 441 ultraviolet detector (254 nm; Waters), and a single sodium iodide crystal flow radioactivity detector. All HPLC chromatograms were recorded by use of a Dynamax dual-channel control–interface module (Rainin) connected to a Macintosh computer (Apple Computer, Inc.) running Dynamax version 1.4 program software. Radioactivity measurements were made by use of a CRC-15R dose calibrator (Capintec).

Male CD-1 mice (24.5–28.4 g) and female SCID mice (18–20 g) were obtained from Charles River Laboratories, Inc. The MCF-7 and MDA-MB-231 cell lines were obtained from Zaver Bhujwalla. All in vivo experimental procedures were undertaken in compliance with U.S. laws governing animal experimentation and were approved by the Johns Hopkins University Animal Care and Use Committee.

(*S*)-2-(1-*tert*-Butoxycarbonyl-2-{4-[2-(5-Methyl-2-Phenyloxazol-4-yl)Ethoxy]Phenyl}Ethylamino)Benzoic Acid Methyl Ester (Compound 2)

A suspension of compound 1 (174.6 mg, 0.349 mmol) in toluene (6 mL) was heated at 80°C for 5 min until a solution formed. To this solution was added DMF di-*tert*-butyl acetal (0.7 mL, 2.92 mmol), and the solution was stirred at 80°C for 30 min before an additional 0.7 mL of the acetal was added. The solution was concentrated under reduced pressure; this step was followed by flash chromatography on silica gel. Product 2 was eluted with 20% ethyl acetate (EtOAc) in hexane (138.3 mg, 71%). ^{1}H nuclear magnetic resonance (NMR) data were as follows: ($CDCl_3$, 300 MHz) δ 7.96–7.99 (m, 2H), 8.17 (d, 1H, J = 7.4), 7.90 (dd, 1H, J = 8.0, 1.5 Hz), 7.39–7.46 (m, 3H), 7.29 (m, 1H), 7.15 (dm, 1H, J = 8.8 Hz), 6.82 (dm, 1H, J = 8.7 Hz), 6.56–6.63 (m, 2H), 4.19–4.26 (m, 3H), 3.85 (s, 3H), 3.01–3.15 (m, 2H), 2.36 (s, 3H), and 1.35 (s, 9H). ^{13}C NMR data were as follows: ($CDCl_3$, 75.47 MHz) δ 171.57, 168.53, 159.35, 157.62, 149.62, 144.88, 134.28, 132.63, 131.69, 130.36, 129.64, 128.71, 128.55, 127.71, 125.81, 115.27, 114.37, 111.52, 110.88, 81.55, 66.59, 58.04, 51.41, 37.78, 27.83, 26.28, and 10.12; M^+ = 557 Da.

(*S*)-2-(1-*tert*-Butoxycarbonyl-2-{4-[2-(5-Methyl-2-Phenyloxazol-4-yl)Ethoxy]Phenyl}Ethylamino)Benzoic Acid (Compound 3)

To a suspension of compound 2 (69.2 mg, 0.124 mmol) in dioxane (1.0 mL) was added NaOH (1 mol/L, 0.25 mL); the resulting solution was stirred at ambient temperature for 50 h under nitrogen. The solution was diluted with 15 mL of water and neutralized with 0.5 mL of HCl (1 mol/L). The resulting white oil was extracted three times with diethyl ether (Et_2O). The combined Et_2O layers were washed with water and then with brine, dried over $MgSO_4$, and concentrated under reduced pressure. The resulting clear oil was applied to a silica gel column that had been washed with 25% EtOAc in hexane plus 1% acetic acid; this step was followed by elution of the product with 100% EtOAc plus 1% acetic acid (32.3 mg, 48%). ^{1}H NMR data were as follows: ($CDCl_3$, 300 MHz) δ 7.95 (d, 4H, J = 1.9 Hz), 7.40 (s, 2H), 7.34 (t, 1H, J = 1.5 Hz), 7.34 (t, 1H, J = 1.5 Hz), 7.13 (d, 2H, J = 8.8 Hz), 6.83 (d, 2H, J = 8.8 Hz), 6.60 (q, 2H, J = 9.4 Hz), 4.21 (t, 4H, J = 7.1 Hz), 3.08 (t, 2H, J = 7.0 Hz), 2.96 (t, 2H, J = 6.6 Hz), 2.35 (4H), 2.11 (s, 4H), and 1.37 (s, 9H). ^{13}C NMR data were as follows: ($CDCl_3$, 77.27 MHz) δ 171.86, 162.98, 159.72, 157.92, 150.51, 145.35, 135.32, 132.90, 132.80, 130.76, 130.06, 128.91, 128.79, 127.84, 126.17, 115.70, 114.84, 111.91, 110.39, 82.00, 66.94, 58.26, 37.94, 28.15, 26.42, and 10.47; M^+ = 543 Da.

^{11}C-Compound 1

Compound 3 (0.66 mg, 1.2 μmol) in 200 μL of DMF was added to 0.8 mg (2.5 μmol) of cesium carbonate. The precursor solution was cooled to −42°C, and ^{11}C-methyl iodide was bubbled into the solution until the radioactivity reached a plateau. The vial was removed from the dry ice bath and heated in an 80°C water bath for 3 min. The reaction mixture was diluted with 200 μL of 95:5 (v/v) acetonitrile:water and injected into the semipreparative HPLC system described above. The mixture was eluted from the column (C_{18} Econosil, 10 × 250 mm; Alltech) with 95:5 (v/v) acetonitrile:water at a flow rate of 10 mL/min. The sample with a radioactive peak corresponding to ^{11}C-compound 2 (retention time, 4.7 min) was collected in a rotary evaporator modified for remote addition and removal of solutions. The HPLC solvent was evaporated to dryness at 80°C under vacuum. After evaporation, the residue was dissolved in 200 μL of trifluoroacetic acid (TFA), and the mixture was heated at 80°C for 2 min at atmospheric pressure to cleave the *tert*-butyl ester. After 2 min, the TFA was evaporated under vacuum. The residue was dissolved in 3.0 mL of 8.4% sterile sodium bicarbonate solution and then diluted with 1.0 mL of ethanol and 6.0 mL of sterile saline. The solution was remotely passed through a 0.2-μm Millex GV sterile filter (Millipore) into a sterile, pyrogen-free bottle.

A 100-μL sample of the final product was injected into an analytic C_{18} Econosil HPLC column (4.6 × 250 mm; Alltech) and eluted with 60:40 (v/v) acetonitrile:water (ammonium formate at 0.1 mol/L) at a flow rate of 4 mL/min. The radioactive peak sample corresponding to ^{11}C-compound 1 (retention time, 1.6 min) coeluted with a standard sample.

Biodistribution of ^{11}C-Compound 1 in Mice

We used CD-1 mice to delineate the normal tissue distribution of the radiotracer and SCID mice harboring breast tumor xenografts to determine target (tumor)-to-nontarget (muscle) uptake ratios. SCID mice were also used to test the binding specificity of ^{11}C-compound 1 through receptor blockade because only the SCID mice would have the most salient target tissue, that is, tumor. We did not expect any significant difference in the pharmacokinetics of ^{11}C-compound 1 between the 2 strains of mice.

Normal, nonfasting male CD-1 mice were injected via the tail vein with 6.03 MBq (163 μCi, 2.55 μg/kg) of ^{11}C-compound 1. Three mice each were sacrificed by cervical dislocation at 5, 15, 30, 60, and 90 min after injection. The liver, kidneys, small intestine, pancreas, bladder, muscle, brain, and a fat pad were removed quickly and placed on ice. A 0.1-mL sample of blood also was collected. The organs were weighed, and the tissue radioactivity was measured with an automated γ-counter (1282 Compugamma CS; Pharmacia/LKB Nuclear, Inc.). The percentage injected dose per gram of tissue (%ID/g) was calculated by comparison with samples of a standard dilution of the initial dose. All measurements were corrected for decay.

Tumor Uptake of ^{11}C-Compound 1

Female SCID mice ($n = 8$) were implanted in the neck scruff with an estradiol pellet that released 1.7 mg over 60 d (Innovative Research of America) 2 d before inoculation with cancer cells. Mice were inoculated in the left flank with 3×10^6 MCF-7 cells in 100 μL of Matrigel (Becton Dickenson) by subcutaneous injection. After 4 wk of tumor growth (mean diameter, approximately 7 mm), analysis of the biodistribution of ^{11}C-compound 1 was performed. Mice were injected via the tail vein with 10.5 MBq (283 μCi, 0.235 μg/kg) of ^{11}C-compound 1. To assess for the specificity of binding to PPARγ, 3 of the mice were given unlabeled compound 1 at 2 mg/kg, coinjected with the radiotracer. The mice were sacrificed at 30 or 60 min after injection of the radiotracer. The liver, kidneys, muscle, and tumor were removed quickly and placed on ice. A 0.1-mL sample of blood also was collected. All tissue samples were processed as described above.

Advanced Technology Laboratory Animal Scanner (ATLAS) PET of ^{11}C-Compound 1 in Tumor-Bearing Mice

Two female SCID mice, each bearing an MDA-MB-231 human breast carcinoma xenograft (4–5 mm in diameter) in the mammary fat pad, were anesthetized by intraperitoneal administration of a combination of ketamine (72 mg/kg), xylazine (6 mg/kg), and acepromazine (6 mg/kg). One mouse was injected intraperitoneally with unlabeled compound 1 at 2 mg/kg. Unlabeled compound 1 was prepared as a stock solution (0.18 mg/mL) in 10% (w/v) hydroxypropyl-β-cyclodextrin in water immediately before use. After 30 min, both mice were injected via the tail vein with 7.4 MBq (200 μCi, 4.0 pg) of ^{11}C-compound 1 in 200 μL of saline. The mice were positioned side by side on the bed of an ATLAS small-animal PET scanner (PET Department, National Institutes of Health) and kept anesthetized with isoflurane (0.5%–1%; approximately 1 L/min). The mice were imaged at 1 h after injection with a 10-min static scan. After the PET image was acquired, the ATLAS gantry and mice were removed and placed inside an X-SPECT scanner (Gamma Medica) for small-animal CT image acquisition. CT images were acquired with 360° rotation at 50 mV and were reconstructed by use of commercial software (Gamma Medica).

PPARγ Expression in Mouse Tissues and Xenografts

Two female SCID mice, 1 bearing a subcutaneous MDA-MB-231 xenograft and 1 bearing an orthotopic MCF-7 xenograft, were sacrificed when their tumors reached 0.5–0.7 mm in diameter. Samples of muscle, white fat, spleen, gallbladder, small intestine, large intestine, and the MCF-7 tumor were harvested from 1 mouse. The MDA-MB-231 tumor was harvested from the other mouse. The samples were weighed quickly, minced, and placed in sterile 1.5-mL microcentrifuge tubes. A clean steel pestle was used to grind the tissues into a pulp before the addition of 500 μL of lysis buffer (pH 7.5; 10% sodium dodecyl sulfate and ethylenediaminetetraacetic acid at 10 mmol/L). The samples were boiled at 95°C for 30 min. After the samples cooled, the cellular debris was pelleted by centrifugation at 16,100*g* for 5 min at an ambient temperature. The supernatants were collected and placed in fresh tubes. Total protein in each tissue extraction was quantitated by use of a DC protein (Bradford) assay (Bio-Rad).

Samples of each tissue lysate (10 μL) were applied directly to a polyvinylidene difluoride membrane (Millipore) as separate lines. Standard glutathione *S*-transferase–PPARγ human fusion protein (NeoMarkers) samples in amounts of 200, 100, 50, 25, and 12.5 ng were applied to the membrane as separate lines. The blot was blocked with 5% dried milk in TBST (Tris at 25 mmol/L [pH 7], NaCl at 150 mmol/L, KCl at 2.7 mmol/L, and 0.05% Tween 20), washed twice with TBST, incubated with a 1:1,000 dilution of anti-PPARγ monoclonal antibody (MAB3872; Chemicon International) in TBST for 1 h, and washed twice more with TBST. A 1:3,000 dilution of anti–mouse IgG conjugated to horseradish peroxidase (Amersham) in TBST was applied to the blot, and the blot was incubated for 1 h in the dark and rinsed twice with TBST. The blot then was immersed in 10 mL of 1:1 (v/v) SuperSignal Luminol Enhancer:SuperSignal Peroxide Solution (Pierce) before reading was done with a Typhoon 9210 PhosphorImager (Molecular Dynamics).

The amount of PPARγ in each tissue sample was quantified by drawing regions of interest around each PPARγ-positive spot, including the 5 glutathione *S*-transferase–PPARγ standards spotted onto the blot. These regions of interest were quantified by use of ImageQuant software (Molecular Dynamics). The nanograms of PPARγ per milligram of wet tissue were calculated on the basis of the amount of tissue lysate loaded onto the gel and the mass of tissue from which each lysate was derived.

Metabolism of ^{11}C-Compound 1 in Mice

Three normal, nonfasting male CD-1 mice were injected via the tail vein with 37 MBq (1 mCi) of ^{11}C-compound 1. The mice were sacrificed by decapitation at 15, 30, and 60 min after injection. Plasma from heparinized blood was diluted to 3 mL and added to a solution of urea and citric acid. The liver and spleen were homogenized in acetonitrile and centrifuged. The supernatant was diluted to 3 mL and added to a solution of urea and citric acid. The diluted solutions were analyzed by HPLC. A Strata (Phenomenex) capture column was used with a C_{18} Prodigy (Phenomenex) analytic column, and 70% acetonitrile:30% sodium phosphate buffer (50 mmol/L; pH 2.4) was run at 3 mL/min.

Metabolism of Compound 1 in Human, Rat, and Mouse Liver Homogenates

Compounds were incubated with human, rat, and mouse liver homogenates (S9 fraction). Pooled human, rat, and mouse liver S9 homogenates were purchased from XenoTech. Reaction mixtures for metabolic stability studies consisted of pooled liver S9 homogenates (final protein concentration, 5 mg/mL), compound 1 (final concentration, 1 μmol/L, as a free base prepared in dimethyl sulfoxide to maintain a final dimethyl sulfoxide concentration of <1%), uridine 5′-diphosphate-glucuronic acid at 5 mmol/L, reduced nicotinamide adenine dinucleotide phosphate (NADPH) at 2 mmol/L, and $MgCl_2$ at 10 mmol/L in a final volume of 0.5 mL of potassium phosphate buffer (75 mmol/L; pH 7.4). Incubation mixtures in 96-well polypropylene (2-mL) plates were placed into a shaking incubator maintained at 37°C before the addition of NADPH. An initial-time-point sample was collected immediately after the addition of NADPH, and subsequent samples were collected at 15, 30, and 60 min. Each reaction was terminated by transferring samples of incubation mixtures (0.1 mL) into acetonitrile (0.2 mL) maintained at 4°C. Precipitated protein was removed by centrifugation (2,600 relative centrifugal force (rcf) for 15 min), and the resultant supernatant was transferred to a new 96-well polypropylene deep-well plate for subsequent analysis by liquid chromatography–tandem mass spectrometry. Drug-free matrix control samples and quality control standards were included in each run and treated in the same manner as unknown samples. Samples were analyzed by use of a series 1100 HPLC system

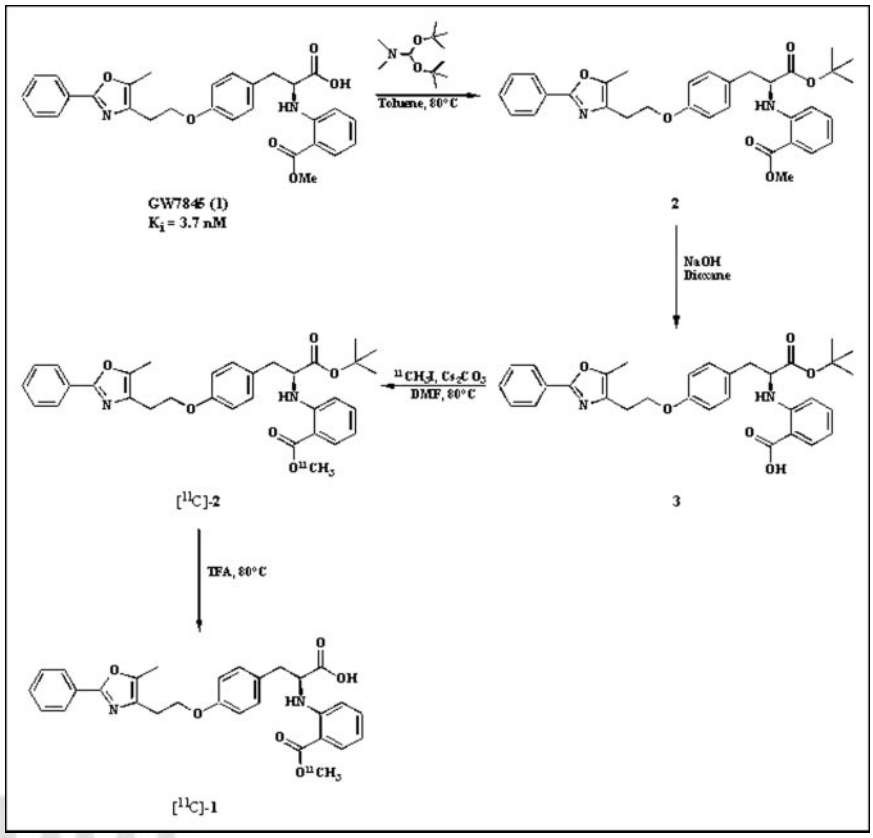

FIGURE 1. Synthesis of ^{11}C-compound 1. OMe = methoxy (OCH_3); K_i = inhibitor constant.

(Agilent) interfaced with a Sciex API3000 (Perkin-Elmer) liquid chromatography–tandem mass spectrometry apparatus (Turbospray ion source). We performed this study once, which is the industry standard, and found that the confidence limits on the data were on the order of ±15% those for studies performed multiple times.

RESULTS

We used a simple strategy to produce ^{11}C-compound 1, that is, to replace the methyl ester of compound 1 with a ^{11}C-methyl group. To do so, we were first required to protect the 1-carboxyl group of compound 1 before demethylation of the benzoic acid ester to ensure the regioselectivity of the ensuing ^{11}C-methylation procedure (Fig. 1). Compound 1 was reacted with DMF di-*tert*-butyl acetal to provide compound 2 at a 71% yield. Compound 2 then could be deprotected under basic conditions to provide compound 3 at a 48% yield; this compound was the immediate precursor for methylation with ^{11}C-methyl iodide.

^{11}C-Compound 1 was synthesized by reacting a *tert*-butyl-protected carboxy precursor with ^{11}C-methyl iodide in the presence of a cesium carbonate base. The intermediate, ^{11}C-compound 2, was purified by semipreparative HPLC. Attempts to hydrolyze the *tert*-butyl-protecting group in a variety of solvents before HPLC purification were unsuccessful. Removal of the *tert*-butyl-protecting group finally was achieved by treatment with neat TFA. Chemical purity, radiochemical purity, and specific activity were all determined by analytic HPLC. Specific radioactivity was calculated by comparing the area of the ultraviolet absorbance peak of the carrier ligand in a sample of known radioactivity with the area of a standard sample. The specific radioactivity was 1,222 GBq/μmol (33,024 mCi/μmol; $n = 6$) at the end of synthesis. The mean ± SD radiochemical yield was 8% ± 4% (uncorrected for decay). The final formulation was determined by analytic HPLC to be >99% pure. No ^{11}C-compound 2 was detected in the final formulation.

The kinetics of biodistribution of ^{11}C-compound 1 in mouse liver, kidneys, small intestine, pancreas, blood, bladder, muscle, fat, and brain after intravenous injection of the radiotracer were determined. Table 1 shows the decay-corrected %ID/g data for all organs and time points. ^{11}C-Compound 1 showed a high initial level of uptake in the liver that rapidly washed out over 30 min. After 60 min, the highest level of uptake was observed in the liver and kidneys. This finding differs from those for the known target sites (spleen, white fat, and intestine) of PPARγ measured in rats (*11*). Despite the high lipophilicity of this compound (ClogP = 5.63, as calculated by ChemDraw [CambridgeSoft]), there was generally less than 1 %ID/g of uptake in the brain.

In normal SCID mice, the spleen, a target organ for PPARγ (*10*), displayed a relatively high level of uptake (3.00 %ID/g), with spleen-to-heart and spleen-to-muscle uptake ratios of 1.8 and 3.1, respectively (Table 2). Very

TABLE 1
Tissue Distribution of ^{11}C-Compound 1 in Normal Male CD-1 Mice

Tissue	Mean ± SD (n = 3) %ID/g at:				
	5 min	15 min	30 min	60 min	90 min
Liver	27.23 ± 7.60	13.95 ± 7.13	8.51 ± 4.73	8.45 ± 0.06	5.75 ± 2.15
Kidneys	6.16 ± 2.35	3.72 ± 1.80	7.53 ± 7.28	7.99 ± 6.67	2.08 ± 0.73
Small intestine	2.86 ± 1.48	4.93 ± 3.78	6.73 ± 4.46	5.12 ± 0.06	3.59 ± 0.70
Pancreas	2.28 ± 1.34	0.90 ± 0.74	4.36 ± 2.48	3.78 ± 0.95	2.74 ± 1.19
Blood	8.55 ± 3.15	3.69 ± 2.14	2.77 ± 1.48	2.95 ± 0.09	1.81 ± 0.73
Bladder	3.06 ± 2.26	0.73 ± 0.66	1.66 ± 1.43	2.93 ± 2.71	1.85 ± 0.39
Muscle	1.02 ± 0.56	1.74 ± 1.78	0.94 ± 0.41	1.39 ± 1.96	0.82 ± 0.44
Fat	1.82 ± 1.59	0.85 ± 0.44	1.22 ± 0.90	1.12 ± 0.83	1.21 ± 0.52
Brain	1.30 ± 0.18	0.94 ± 0.54	0.89 ± 0.48	0.99 ± 0.08	0.55 ± 0.19

high levels of duodenal uptake (7 %ID/g) and gallbladder uptake (127 %ID/g) likely reflect the enterohepatic metabolism of the lipophilic compound. Attempted blockade of PPARγ by pretreatment of the animals with unlabeled compound 1 at 2 mg/kg failed to decrease radiotracer binding to the expected target tissues, that is, spleen, white fat, and intestine (*10,11*). SCID mice bearing MCF-7 xenografts were used to determine the specificity of ^{11}C-compound 1 uptake, as MCF-7 cells are known to express elevated levels of PPARγ (*12*). At 60 min after injection, the tumor-to-muscle uptake ratio was 1.5 (Fig. 2). Attempted blockade by coinjection of unlabeled compound 1 at 2 mg/kg again failed to decrease radiotracer binding. In fact, coinjection of the blocker produced a trend toward increased uptake of ^{11}C-compound 1 in all tissues except for the liver.

PET analysis of ^{11}C-compound 1 was performed with SCID mice bearing MDA-MB-231 tumors (Fig. 3A). The locations of the tumors could not be identified as independent from surrounding soft tissue on the PET images alone. CT immediately after PET was required to define the locations of the tumors (Fig. 3B). Attempted blockade of ^{11}C-compound 1 within tumors with unlabeled compound 1 failed to demonstrate receptor-mediated tissue uptake, supporting the results of the biodistribution study. Enterohepatic metabolism was confirmed by the high levels of liver and gallbladder uptake of ^{11}C-compound 1.

Quantification of PPARγ protein in selected mouse tissues and in MDA-MB-231 and MCF-7 tumor xenografts was performed by a dot–blot assay (Table 3). Both nanograms of PPARγ per milligram of wet tissue and nanograms of PPARγ per microgram of total protein are reported. The results indicate that both the MDA-MB-231 and the MCF-7 xenografts used in this study contained only modest levels of PPARγ protein relative to the other tissues that were sampled (muscle, white fat, spleen, gallbladder, small intestine, and large intestine). The spleen and gallbladder contained the highest levels of the receptor (11.58 and 11.87 ng/μg of total protein, respectively), whereas the 2 xenografts contained less receptor than did muscle (muscle, 7.03 ng/μg of total protein; MCF-7 xenograft, 4.20 ng/μg of total protein; and MDA-MB-231 xenograft, 4.82 ng/μg of total

TABLE 2
Tissue Distribution of ^{11}C-Compound 1 in Normal Female SCID Mice

Tissue	%ID/g	
	Control*	Blocked†
Blood	3.22 ± 0.36	3.14 ± 0.42
Spleen	3.00 ± 0.27	3.46 ± 0.67
Liver	10.18 ± 0.88	10.76 ± 0.52
White fat	3.57 ± 0.46	4.41 ± 1.01
Gallbladder	126.18 ± 62.93	71.77 ± 33.41
Kidneys	2.99 ± 0.09	3.36 ± 0.28
Lungs	2.31 ± 0.59	2.01 ± 0.29
Heart	1.65 ± 0.14	1.73 ± 0.19
Muscle	0.98 ± 0.18	1.17 ± 0.24
Duodenum	7.04 ± 2.45	5.21 ± 1.84
Ileum	2.03 ± 0.25	2.18 ± 0.33

*At 60 min after injection (n = 4).
†After intraperitoneal injection of compound 1 at 2 mg/kg 30 min before tracer.

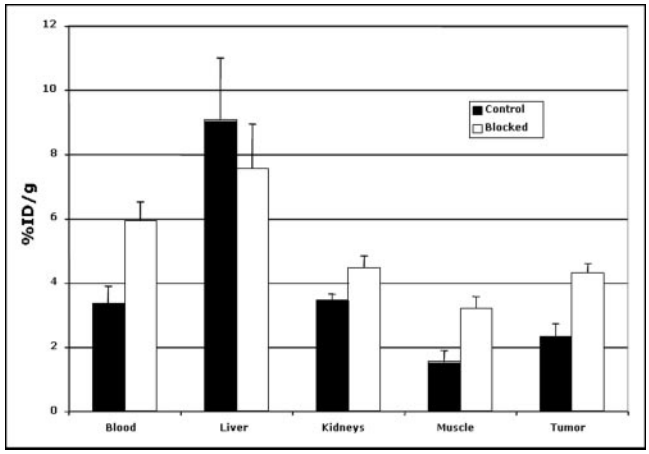

FIGURE 2. Binding selectivity of ^{11}C-compound 1 at 60 min after injection (n = 3) in female SCID mice bearing MCF-7 tumors. Tissue distribution of ^{11}C-compound 1 upon coinjection with unlabeled compound 1 at 2 mg/kg showed either equal or increased tracer uptake. Error bars indicate SDs.

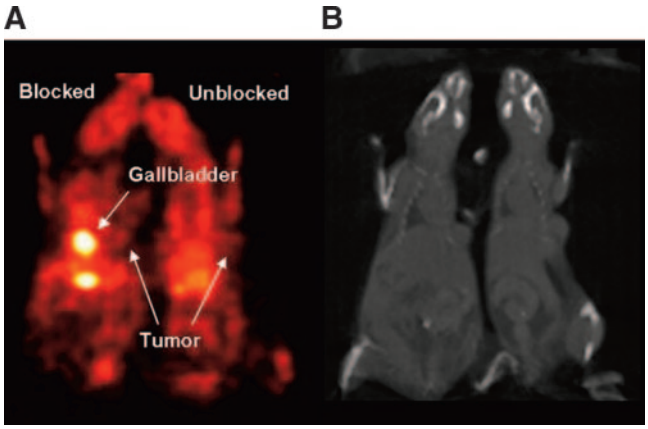

FIGURE 3. (A) PET image showing in vivo distribution of ^{11}C-compound 1 at 60 min after injection in SCID mice bearing MDA-MB-231 tumors. Tissue distribution of ^{11}C-compound 1 after intraperitoneal administration of unlabeled compound 1 at 2 mg/kg showed either equal or increased tracer uptake. (B) CT image of same mice.

protein). These results do not parallel the ^{11}C-compound 1 distribution data in mice (Tables 1 and 2), suggesting that radiopharmaceutical uptake may be independent of PPARγ expression.

A metabolite assay was performed for plasma, liver, and spleen. The results (Table 4) indicate that >76% of ^{11}C-compound 1 was metabolized after 15 min. A slight decrease in the observed percentage of metabolized ligand at later time points probably was attributable to clearance of the radioactive metabolite.

The biodistribution and metabolism results for ^{11}C-compound 1 prompted us to investigate further the metabolism of compound 1 in human, rat, and mouse liver homogenates. For these studies, we used compound 1 at 1 μmol/L, a concentration approximately 300 times that used in the radiotracer uptake study. Significantly less metabolism was observed under these conditions in any of the species tested (Table 5).

DISCUSSION

PPARγ is a ligand-activated transcription factor that induces a variety of genes, including those involved in apoptosis, inhibition of the cell cycle, and antiangiogenesis, all antitumor effects (*13–16*). PPARγ is not, however, a true tumor suppressor, because in some instances its activation can be procarcinogenic (*15*). Although discovered fairly recently (1990), the PPARs are among the most studied of ligand-activated transcription factors, in part because of their antineoplastic effects, which have been demonstrated not only in tissue cultures but also in vivo in a variety of model systems (*7,13,14,16*). Some results of PPARγ activation studies have been contradictory (*15*), suggesting that studying its effects in vivo would be useful not only in clinical trials for patient segregation (see above) but also in preclinical development for understanding the mechanisms of action of various ligands. For these reasons and because of the encouraging antitumor effects of *N*-aryl tyrosine activators of PPARγ in vivo (*7*), we sought a positron-emitting agonist based on GW7845, compound 1.

Kim et al. synthesized and evaluated in vivo 2 ^{18}F-labeled PPARγ agonists (*10*). The results that we report with ^{11}C-compound 1 are similar to theirs, that is, high levels of radiotracer uptake in organs associated with enterohepatic metabolism and lack of definitive receptor-mediated uptake. However, compared with that earlier report, we observed higher tumor-to-muscle and spleen-to-muscle uptake ratios (1.5 and 3.1, respectively, in mice), suggesting that at least a portion of the radiopharmaceutical uptake demonstrated represents specific binding. Our absolute uptake values tended to be higher as well. The most likely reason for these findings is the higher affinity of tyrosine-benzophenone series than of phenylpropanoic acids (almost 2-fold). Our compound was based on GW7845, which is known to be a highly potent agonist of PPARγ, and was the pure *S*-

TABLE 3
PPARγ Distribution in Selected Mouse Tissues and in MCF-7 and MDA-MB-231 Xenografts

Tissue	ng of PPARγ/mg of wet tissue	ng of PPARγ/μg of total protein
Muscle	13.06	7.03
White fat	5.81	7.27
Spleen	18.70	11.58
Gallbladder	174.72	11.87
Small intestine	8.38	5.09
Large intestine	25.18	6.70
MCF-7	4.86	4.20
MDA-MB-231	4.65	4.82

TABLE 4
Metabolism of ^{11}C-Compound 1 in Normal Male CD-1 Mice

Time (min)	% Metabolized in: Plasma	Liver	Spleen
0	0	0	0
15	87.7	76.1	84.1
30	76.9	86.9	82.4
60	66.9	79.5	71.1

TABLE 5
In Vitro Metabolic Stability of Compound 1 in Liver S9 Homogenates

Time (min)	% Parent drug remaining in the following samples (half-life, min) Human (89)	Rat (>120)	Mouse (112)
0	100	100	100
15	80	90	87
30	72	94	76
60	61	NR	69

enantiomer. In an effort to demonstrate the binding specificity of ^{11}C-compound 1, we coadministered unlabeled compound 1 in 1 set of experiments. That we were unable to block the uptake of ^{11}C-compound 1 in target tissues (spleen and tumor) suggests that most of the radiotracer uptake was attributable to nonspecific binding, a finding that is common for lipophilic compounds. The ClogP of compound 1 was calculated to be 5.63, which is in a range that may be too lipophilic for a successful radiotracer.

A curious finding that Kim et al. (*10*) and we demonstrated was a slight trend toward an increase in radiopharmaceutical uptake on the coadministration of a blocker (Fig. 2). One possible explanation is the saturation not only of PPARγ in the tissues by compound 1 at 2 mg/kg but also of sites involved in its metabolism. The PET images obtained after the administration of a blocker (Fig. 3A) clearly demonstrate an increase in uptake in the gallbladder, liver, and intestine. That finding was not seen in the biodistribution assay for the gallbladder (Table 2) because of sampling error in the dissection and counting of gallbladder radioactivity that would not be evident on the images. Our investigations of the metabolism of both compound 1 at 1 μmol/L in vitro and tracer doses of ^{11}C-compound 1 in vivo indicate that compound 1 undergoes modest metabolism across species in vitro but that ^{11}C-compound 1 undergoes extensive metabolism in vivo. These findings support the notion that at tracer doses, metabolism likely was suppressed by blockade, accounting for the increased radiopharmaceutical uptake in the tissue distribution study in which blockade was used. Note that metabolism likely would have been attributable to hydrolysis of the radioactive methyl ester, so that metabolites accumulating within tissues would not be expected to be radioactive.

In addition to significant nonspecific binding, another reason that tumor uptake was relatively low was the low levels of PPARγ in the tumors tested. Breast cancer cell lines, including MCF-7 cells, are known to have higher PPARγ levels (*17*), 6- to 25-fold (*12*), than are nonmalignant tissues. However, when we quantified the levels of PPARγ in the xenograft lines used here and compared them with the levels found in other mouse tissues, both the MDA-MB-231 and the MCF-7 xenografts contained less PPARγ protein than the other tissues tested (Table 3). Additionally, significant PPARγ protein levels were found in all of the tissues that were tested. This finding suggests that imaging of PPARγ expression in breast malignancies by PET may be difficult.

Further complicating the ligand binding of potential new PPARγ-based radiotracers is that the affinity of such compounds likely depends on the degree of phosphorylation of the receptor (*18*). Concurrent treatment with mitogen-activated protein kinase inhibitors, if nontoxic in vivo, may be another strategy for improving the affinity of potential radioligands for PPARγ.

PPARγ is an inherently challenging target for imaging not only because of its relatively low concentrations in target tissues and the possibility that in some cases the concentrations may be even lower in malignant tissues than in normal tissues (*19,20*) but also because 1 known target tissue is adipose. Naturally, ligands that bind to a target in adipose tissue will need to be somewhat lipophilic to gain access to that target. This problem becomes even more significant in the design of imaging agents for breast cancer, an ostensible goal of this study, because much of the normal breast is composed of fat.

CONCLUSION

Although we demonstrated a better than 1:1 tumor-to-muscle uptake ratio for ^{11}C-compound 1 and increased uptake in 1 target tissue (spleen), the majority of the radiopharmaceutical uptake that we observed likely was attributable to nonspecific binding. Because of the high receptor-binding affinity of compound 1, further structural modification of the tyrosine-benzophenone series, in which the *N*-aryl moiety has proved to be tolerant of substitution with a variety of functions that can help decrease lipophilicity, may lead to a successful PPARγ-based imaging agent for PET.

ACKNOWLEDGMENTS

This work was supported by National Institutes of Health grants CA92871 and CA103175. The authors thank Zaver Bhujwalla for helpful discussions, Robert Smoot for assistance with the radiosyntheses, Paige Rauseo for performing the mouse dissections, James Fox for acquiring the small-animal PET and CT images, and John Hilton for performing the radioactive metabolism assay.

REFERENCES

1. Willson TM, Brown PJ, Sternback DD, Henke BR. The PPARs: from orphan receptors to drug discovery. *J Med Chem*. 2000;43:527–550.
2. Ferre P. The biology of peroxisome proliferator-activated receptors: relationship with lipid metabolism and insulin sensitivity. *Diabetes*. 2004;53(suppl 1):S43–S50.
3. Cabrero A, Laguna JC, Vazquez M. Peroxisome proliferator-activated receptors and the control of inflammation. *Curr Drug Targets Inflamm Allergy*. 2002;1:243–248.
4. Yoshimura R, Matsuyama M, Hase T, et al. The effect of peroxisome proliferator-activated receptor-gamma ligand on urological cancer cells. *Int J Mol Med*. 2003;12:861–865.
5. Yue TL. Cardioprotective effects of thiazolidinediones, peroxisome proliferator-activated receptor-gamma agonists. *Drugs Today*. 2003;39:949–960.
6. Kintscher U, Lyon CJ, Law RE. Angiotensin II, PPAR-gamma and atherosclerosis. *Front Biosci*. 2004;9:359–369.
7. Suh N, Wang Y, Williams CR, et al. A new ligand for the peroxisome proliferator-activated receptor-gamma (PPAR-gamma), GW7845, inhibits rat mammary carcinogenesis. *Cancer Res*. 1999;59:5671–5673.
8. Panigrahy D, Shen LQ, Kieran MW, Kaipainen A. Therapeutic potential of thiazolidinediones as anticancer agents. *Expert Opin Investig Drugs*. 2003;12:1925–1937.
9. Cobb JE, Blanchard SG, Boswell EG, et al. N-(2-Benzoylphenyl)-L-tyrosine PPARgamma agonists. 3. Structure-activity relationship and optimization of the N-aryl substituent. *J Med Chem*. 1998;41:5055–5069.
10. Kim SH, Jonson SD, Welch MJ, Katzenellenbogen JA. Fluorine-substituted ligands for the peroxisome proliferator-activated receptor gamma (PPAR-gamma): potential imaging agents for metastatic tumors. *Bioconjug Chem*. 2001;12:439–450.
11. Braissant O, Foufelle F, Scotto C, Dauca M, Wahli W. Differential expression of

peroxisome proliferator-activated receptors (PPARs): tissue distribution of PPAR-alpha, -beta, and -gamma in the adult rat. *Endocrinology*. 1996;137:354–366.
12. Nwankwo JO, Robbins ME. Peroxisome proliferator-activated receptor-gamma expression in human malignant and normal brain, breast and prostate-derived cells. *Prostaglandins Leukot Essent Fatty Acids*. 2001;64:241–245.
13. Grommes C, Landreth GE, Schlegel U, Heneka MT. The nonthiazolidinedione tyrosine-based peroxisome proliferator-activated receptor gamma ligand GW7845 induces apoptosis and limits migration and invasion of rat and human glioma cells. *J Pharmacol Exp Ther*. 2005;313:806–813.
14. Keshamouni VG, Arenberg DA, Reddy RC, et al. PPAR-gamma activation inhibits angiogenesis by blocking ELR+CXC chemokine production in non-small cell lung cancer. *Neoplasia*. 2005;7:294–301.
15. Michalik L, Desvergne B, Wahli W. Peroxisome-proliferator-activated receptors and cancers: complex stories. *Nat Rev Cancer*. 2004;4:61–70.
16. Alarcon de la Lastra C, Sanchez-Fidalgo S, Villegas I, Motilva V. New pharmacological perspectives and therapeutic potential of PPAR-gamma agonists. *Curr Pharm Des*. 2004;10:3505–3524.
17. Mueller E, Sarraf P, Tontonoz P, et al. Terminal differentiation of human breast cancer through PPAR gamma. *Mol Cell*. 1998;1:465–470.
18. Shao D, Rangwala SM, Bailey ST, Krakow SL, Reginato MJ, Lazar MA. Interdomain communication regulating ligand binding by PPAR-gamma. *Nature*. 1998;396:377–380.
19. Jiang WG, Redfern A, Bryce RP, Mansel RE. Peroxisome proliferator activated receptor-gamma (PPAR-gamma) mediates the action of gamma linolenic acid in breast cancer cells. *Prostaglandins Leukot Essent Fatty Acids*. 2000;62:119–127.
20. Jiang WG, Douglas-Jones A, Mansel RE. Expression of peroxisome-proliferator activated receptor-gamma (PPARgamma) and the PPARgamma coactivator, PGC-1, in human breast cancer correlates with clinical outcomes. *Int J Cancer*. 2003;106:752–757.